Theoretical Investigation and Structural Optimization of Single-Electrode Triboelectric Nanogenerators

Simiao Niu, Ying Liu, Sihong Wang, Long Lin, Yu Sheng Zhou, Youfan Hu, and Zhong Lin Wang*

Single-electrode triboelectric nanogenerators (SETENGs) significantly expand the application of triboelectric nanogenerators in various circumstances, such as touch-pad technologies. In this work, a theoretical model of SETENGs is presented with in-depth interpretation and analysis of their working principle. Electrostatic shield effect from the primary electrode is the main consideration in the design of such SETENGs. On the basis of this analysis, the impacts of two important structural parameters, that is, the electrode gap distance and the area size, on the output performance are theoretically investigated. An optimized electrode gap distance and an optimized area size are observed to provide a maximum transit output power. Parallel connection of multiple SETENGs with micro-scale size and relatively larger spacing should be utilized as the scaling-up strategy. The discussion of the basic working principle and the influence of structural parameters on the whole performance of the device can serve as an important guidance for rational design of the device structure towards the optimum output in specific applications.

1. Introduction

A rapid growing demand of portable electronic devices and wireless sensor networks has spured great interest in robust and independent energy harvesting techniques. Therefore, scavenging mechanical energy from the ambient environment has attracted worldwide attention due to the universal availability of the mechanical energy, such as vibration and friction. Among all mechanical energy harvesting technologies, triboelectric nanogenerators (TENGs), which are recently invented based on coupling of contact electrification[1–3] and electrostatic induction, show prospect of a promising technology due to their numerous advantages: high output power, high energy conversion efficiency, and inexpensive fabrication.[4–9] However, traditional paired-electrode structured TENGs[4–6,8–10] require one electrode and the corresponding lead to be attached

to the moving part of the devices, which limits their applicability as both energy harvester[4–6,8,9] and self-powered sensors.[10] To overcome this drawback, a new structure of TENGs that eliminates the moving electrode has been experimentally demonstrated. In this structure, only one electrode is attached to (or serves as) the triboelectric layer. The other electrode serves as an electric potential reference and can be placed anywhere in the space, even directly be the ground. Therefore, it is called single-electrode triboelectric nanogenerator (SETENG).[11,12] Although the basic function of SETENGs has been demonstrated, there still lacks a theoretical model to systematically provide an in-depth understanding of their working principle. Further, the influence of their structural parameters on their performance is not clear yet, which, however, is essential for the optimization of their output characteristics.

In this paper, a comprehensive theoretical model is developed for SETENGs. We systematically studied its real time output characteristics utilizing different numerical calculation methods. Based on these results, we clarified the working principle of SETENGs by modeling it as a three-capacitance equivalent circuit. Finally, we investigated the impact of electrode gap distance and area size on the performance of SETENGs and provided strategies for their structural optimization.

2. Contact-separation mode SETENGs

2.1. Conductor-to-Dielectric Contact-Separation Mode SETENGs

We first take the conductor-to-dielectric contact-separation mode SETENGs as an example. Their finite element model was built in 2-Dimensional to simplify the numerical calculation without losing its inherent physics meaning, as shown in **Figure 1**a. One dielectric plate and one metal electrode (primary electrode) are stacked face to face to form the triboelectric pair, with the same length of l and width of w. The thickness is d_0 for Dielectric 1 and d_m for the primary electrode. As one typical configuration, the reference electrode of the same geometric size locates underneath the primary electrode, with a gap of g. The two electrodes are fixed and Dielectric 1 can move along the vertical direction under external mechanical force, with the distance between the two triboelectric layers defined as x. As

S. Niu, Y. Liu, S. Wang, L. Lin, Y. S. Zhou,
Dr. Y. Hu, Prof. Z. L. Wang
School of Materials Science and Engineering
Georgia Institute of Technology
Atlanta, GA 30332–0245, USA
E-mail: zhong.wang@mse.gatech.edu
Prof. Z. L. Wang
Beijing Institute of Nanoenergy and Nanosystems
Chinese Academy of Sciences
Beijing, China

ADVANCED
FUNCTIONAL
MATERIALS
www.afm-journal.de
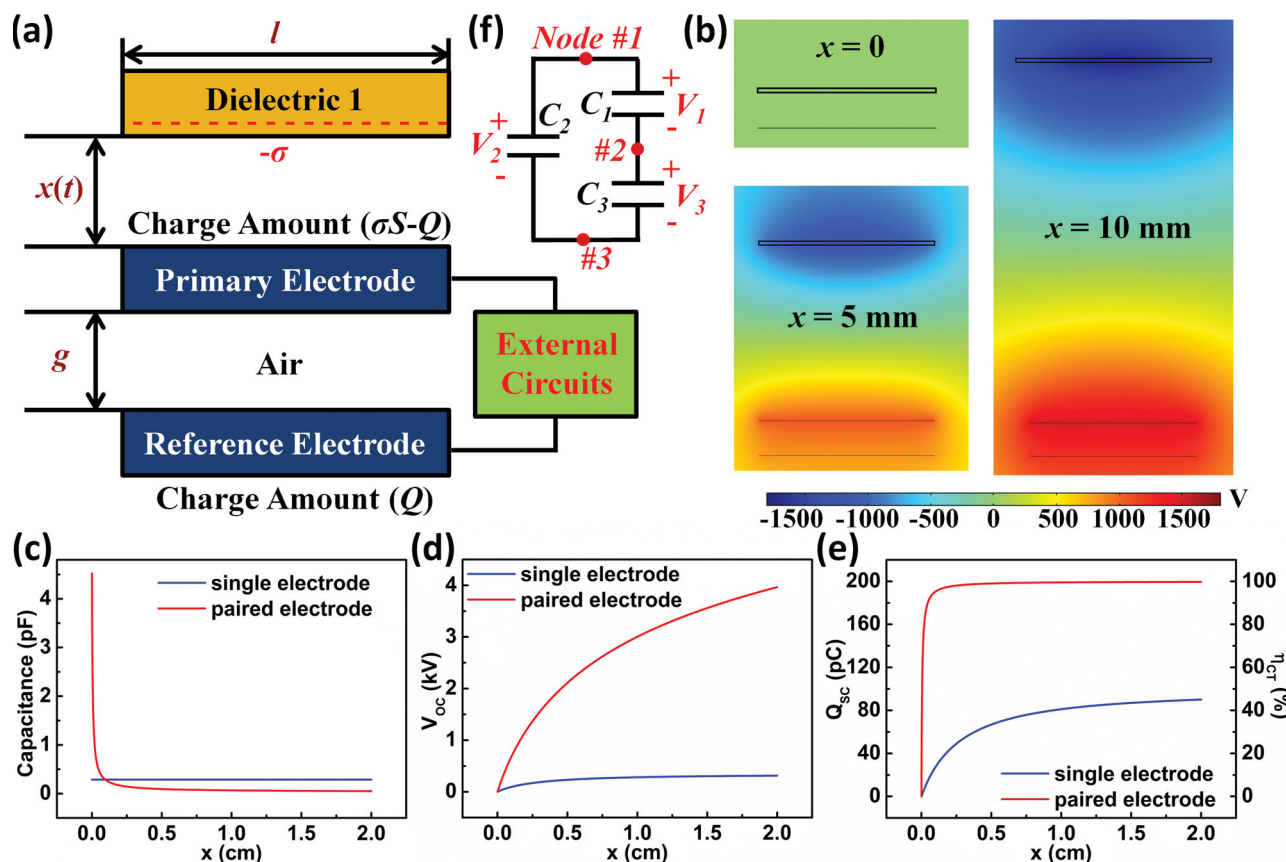
Materials
Views
www.MaterialsViews.com

Figure 1. Basic output characteristics of conductor-to-dielectric contact-mode SETENGs. a) Structure of the FEM model. b) Calculated electric potential distribution at different moving distances x . c–e) Calculated c) capacitance between the two electrodes, d) open circuit voltage, and e) transferred charges at short circuit condition of SETENGs at different x, together with comparison with results of paired electrode TENGs. f) Equivalent circuit model containing three capacitances for the SETENGs under open-circuit (OC) condition.

a result of contact-electrification with the primary electrode, Dielectric 1 carries net negative charges with a density of $-\sigma$ on its bottom surface. Considering the excellent insulation properties of the polymer and the nature of contact electrification, it can be assumed that the charges are uniformly distributed on the surface at macro scale with negligible decay.[13,14] At the same time, there will be equal amount (σwl) of positive charges injected to the primary electrode through contact electrification. With Q defined as the transferred charges from the primary electrode to the reference electrode, the total amount of charges at the primary electrode and reference electrode are $\sigma wl\text{-}Q$ and Q, respectively. The entire structure was surrounded with air, as the usual case in the experiments. The potential at infinity was chosen as the reference point. With the above model, the electric potential distribution in the open circuit (OC) condition ($Q = 0$) with variable separation distances was calculated utilizing COMSOL software. The parameters used in this simulation are listed in **Table 1**. As shown in Figure 1b, due to the electrostatic induction, the electric potential at the primary electrode is higher than that of the reference electrode, which provides the driving force for electrons to flow from the reference electrode to the primary electrode through the external load.

To further understand the output characteristics of the SETENG, its V–Q–x relationship[15] is systematically investigated.

In this regard, its voltage output (V) at different Q and different x is calculated and shown in Figure S1, Supporting Information. Similar to all the other types of TENGs,[15,16] at constant x, V, and Q show an accurate linear relationship, which is because of the capacitor formed between the electrodes. The slope of the V–Q curve is the reciprocal value of the capacitance (C) between the two electrodes. Besides, a non-zero intercept of V-axis (V_{OC}) is observed, which reflects the separation of tribo-charges. Therefore, its V–Q–x relationship can be given as:

Table 1. Utilized parameters in the calculation of SETENG's output characteristics.

Dielectric 1	$\varepsilon_{r1} = 2$, $d_1 = 100$ μm
Thickness of electrodes d_m	1 μm
Width of the structrue w	5 mm
Length of Dielectrics l	5 mm
Gap distance between electrodes g	1 mm
Tribo-charge surface density σ	8 μC m^{-2}
Maximum separation distance x_{max}	0.02 m
Average Velocity v	1 m/s

$$V = -\frac{1}{C} \times Q + V_{OC} \tag{1}$$

V_{OC} and C at different x can be extracted from the intercept and the slope of the linear fitting of the V–Q curves, which is shown in Table S1, Supporting Information. To obtain the approximate equation of V_{OC} in the entire region of x, a second-time interpolation (continuous fraction interpolation method) was carried out. The standard continuous fraction method equation is shown below,[17] with the interpolation parameters listed in Table S2, Supporting Information.

$$V_{OC}(x) = a_1 + \cfrac{x - x_1}{a_2 + \cfrac{x - x_2}{a_3 + \cdots + \cfrac{x - x_{10}}{a_{11}}}} \tag{2}$$

At the short circuit (SC) condition, V equals to 0 and Q equals to the short circuit transferred charges (Q_{SC}). If this condition is applied to Equation 1, the relationship among Q_{SC}, C, and V_{OC} can be obtained as below.

$$0 = -\frac{1}{C} \times Q_{SC} + V_{OC} \tag{3}$$

$$Q_{SC} = V_{OC}C \tag{4}$$

The FEM calculation results of C, V_{OC}, and Q_{SC} for the contact-mode SETENG are plotted in Figure 1c–e, in comparison with the corresponding results of the paired electrode contact-mode TENG with the same size.[16] Their characteristics are completely different. First, due to the fixture of the SETENG's electrodes, its C is nearly a constant (C_0) with the increase of x. However, for the paired electrode structure, its C decreases quickly when the distance between the two electrodes is increasing. Second, in the SETENG, its V_{OC} quickly gets saturated at a value much lower than that of the paired electrode structure. This is because when Dielectric 1 is far away from the electrodes, the influence of Dielectric 1 on the electric field distribution around the electrodes is little. Therefore, further increase in x will contribute little to the increase of V_{OC}. Finally, in the SETENG, Q_{SC} slowly reached its saturation value, which is only half of the value for the paired-electrode structured TENG. When Dielectric 1 is far away from the electrodes, the tribo-charges generated are equally distributed between the two electrodes to maintain the two electrodes at the same electric potential. With the charge transfer efficiency (η_{CT}) defined as the ratio between Q_{SC} and the amount of the tribo-charges, the maximized η_{CT} can only reach 50%, while η_{CT} for the paired-electrode structured TENGs can reach nearly 100% even when x is relatively small.

The above results can be thoroughly understood by a theoretical equivalent circuit model. To build the equivalent circuit model, we need to utilize the concept of nodes. (One node corresponds to a surface/volume with a specific electric potential in an electrostatic system.) For the above system in OC condition, the electric potential across the whole bottom surface of Dielectric 1 is nearly constant, as shown in the FEM calculation

results. Thus, the whole surface can be thought as a node (Node 1). Similarly, the primary electrode and the reference electrode also serve as two nodes, which can be named as Node 2 and Node 3, respectively. Since every two nodes are connected by electric field lines, an equivalent capacitance is formed between each of them. Therefore, the whole electrostatic system can be represented by an equivalent circuit containing three "virtual" capacitors, as shown in Figure 1f. Their capacitances C_1, C_2, and C_3 in the equivalent circuit only represent the capacitive effects from the direct electric line connection between every two nodes without crossing any charged objects (without electrostatic shield of the third object), so they are not actual capacitances that reflects all the electric line connection (both direct and non-direct) between the two nodes and can be directly measured. As a quantitative relationship between the two categories of capacitance, the actual capacitance is the combination of these three capacitances. For example, the actual capacitance (C_b) between Node 1 and Node 3 contains two parts: C_2 and the serial connection of C_1 and C_3 that shows the capacitance effect of non-direct electric lines connection through Node 2, as given by:

$$C_b = C_2 + \frac{C_1 C_3}{C_1 + C_3} \tag{5}$$

Similarly, the actual capacitances between Node 1 and Node 2 (C_a) and between Node 2 and Node 3 (C_0) can also be given as below:

$$C_a = C_1 + \frac{C_2 C_3}{C_2 + C_3} \tag{6}$$

$$C_0 = C_3 + \frac{C_1 C_2}{C_1 + C_2} \tag{7}$$

Combining Equation 5–7, the relationship between the virtual capacitance group (C_1, C_2, and C_3) and the actual capacitance group (C_0, C_a, and C_b) can be given by:

$$C_1 = \frac{2C_a C_b C_0 (C_a C_b - C_b C_0 + C_a C_0)}{2C_a C_b C_0 (C_a + C_b + C_0) - C_a^2 C_b^2 - C_a^2 C_0^2 - C_b^2 C_0^2} \tag{8}$$

$$C_2 = \frac{2C_a C_b C_0 (C_a C_b + C_b C_0 - C_a C_0)}{2C_a C_b C_0 (C_a + C_b + C_0) - C_a^2 C_b^2 - C_a^2 C_0^2 - C_b^2 C_0^2} \tag{9}$$

$$C_3 = \frac{2C_a C_b C_0 (-C_a C_b + C_b C_0 + C_a C_0)}{2C_a C_b C_0 (C_a + C_b + C_0) - C_a^2 C_b^2 - C_a^2 C_0^2 - C_b^2 C_0^2} \tag{10}$$

At OC condition, the total charges on Node 1, 2, and 3 are $-\sigma wl$, σwl, and 0, respectively. Thus, from basic characteristics of capacitances and charge conservation on each node, we can obtain the following equations, in which V_i ($i = 1, 2, 3$) is the voltage across C_i, with the positive direction shown in Figure 1f.

$$V_2 = V_1 + V_3 \tag{11}$$

ADVANCED
FUNCTIONAL
MATERIALS
www.afm-journal.de

Materials
Views
www.MaterialsViews.com

FULL PAPER

$$C_2 V_2 + C_1 V_1 = -\sigma wl \tag{12}$$

$$-C_1 V_1 + C_3 V_3 = \sigma wl \tag{13}$$

Combining Equations 11–13, we can obtain the equation for V_3 at OC condition (V_{OC}), as shown below.

$$V_3 = V_{OC} = \frac{\sigma wl C_2}{C_1 C_2 + C_2 C_3 + C_3 C_1} \tag{14}$$

Thus, substituting Equations 7 and 14 into Equation 4, Q_{SC} and η_{CT} can be given as:

$$Q_{SC} = V_{OC} C_0 = \sigma wl \frac{C_2}{C_1 + C_2} \tag{15}$$

$$\eta_{CT} = \frac{Q_{SC}}{\sigma wl} = \frac{C_2}{C_1 + C_2} \tag{16}$$

Equations 14–16 can be utilized to theoretically explain the basic output characteristics of SETENGs. When $x = 0$, C_a goes to infinity while C_b and C_0 become equal with each other. Therefore, from Equations 8–10, C_1 goes to infinity while C_2 and C_3 are equal to $C_0/2$, which is a finite number. (Detailed derivation is shown in Supporting Information, Section 2.) Therefore, both V_{OC} and Q_{SC} are 0. When x approaches to infinity, both C_a and C_b approach to 0 at the same rate. Therefore, both C_1 and C_2 approach to 0 with the ratio of C_1/C_2 approaching to 1. At the same time, C_3 is getting close to C_0. (Detailed derivation is shown in Supporting Information, Section 2.) Thus, the following results can be obtained at infinite x, which is consistent with the conclusions from FEM calculation.

$$V_{OC}(x = \infty) = \frac{\sigma S}{2 C_0} \tag{17a}$$

$$Q_{SC}(x = \infty) = \frac{\sigma S}{2} \tag{17b}$$

$$\eta_{CT}(x = \infty) = \frac{1}{2} \tag{17c}$$

From Equations 14–16, we observe that the capacitance C_2 is critically important for both V_{OC} and Q_{SC}. C_2 represents the portion of the electric lines directly connecting Node 1 and Node 3, without being electrostatically shielded by Node 2. If all the electric lines connections between the reference electrode and Dielectric 1 needs to come through the primary electrode, C_2 will be equal to 0, which will lead to no output from the SETENG.

Besides OC and SC output property, the load property of the SETENG can be calculated by combining its V–Q–x relationship with Ohm's law, which can be shown as the following equation.

$$V = IR = R \frac{dQ}{dt} \tag{18}$$

By substituting Equation 18 into Equation 1, we can obtain that:

$$R \frac{dQ}{dt} = -\frac{1}{C_0} Q + V_{OC}(x) \tag{19}$$

To solve Equation 19, the boundary condition must be specified. A typical experiment case is that when $t = 0$ s, Dielectric 1 has stopped at $x = 0$ position for a long time and is beginning the separation from the primary electrode. The corresponding boundary condition can be given as $Q\ (t = 0) = 0$. Then, Equation 19 can be analytically solved as:

$$Q(t) = \frac{1}{R} e^{-\frac{t}{R C_0}} \int_0^t V_{OC}(x(t)) e^{\frac{t}{R C_0}} dt \tag{20}$$

Then the current output and the voltage output can be given by:

$$I(t) = \frac{dQ}{dt} = \frac{V_{OC}(x(t))}{R} - \frac{1}{R^2 C_0} e^{-\frac{t}{R C_0}} \int_0^t V_{OC}(x(t)) e^{\frac{t}{R C_0}} dt \tag{21}$$

$$V(t) = V_{OC}(x(t)) - \frac{1}{R C_0} e^{-\frac{t}{R C_0}} \int_0^t V_{OC}(x(t)) e^{\frac{t}{R C_0}} dt \tag{22}$$

The output properties can be numerically calculated under an arbitrary moving mode with V_{OC} approximated by Equation 2. As an example, we consider that Dielectric 1 is first moving at constant velocity and then stops at the maximum moving distance x_{max}. Under this condition, the x-t relationship can be shown as:

$$x = vt \left(t < \frac{x_{max}}{v} \right) \tag{23a}$$

$$x = x_{max} \left(t \geq \frac{x_{max}}{v} \right) \tag{23b}$$

Numerical calculation of the real-time output characteristics for a contact-mode SETENG on different load resistances are shown in **Figure 2**. The parameters utilized in this calculation are listed in Table 1. The charge, current, and voltage curves changing with the external resistance is quite similar to the case in paired electrode TENGs.[16] At SC condition, the electron transfers at the maximum speed. With a load resistance R, the charge curve begins to shift downwards compared to the SC curve. The current and voltage peak value are extracted and plotted in Figure 2d, clearly indicating its three-working-region behavior. The optimum resistance for the maximum transit power is also observed. Similar to the paired electrode TENGs, this load-dependence behavior comes from limitation on the real charge transfer rate by the external resistance.[16] At small R (Region I), the limitation effect of charge transfer of the resistor is small and the charge and current curves are close to the SC curve. When R is in the medium level (Region II), that limitation begins to be more and more significant and the curves significantly shift downwards. When R is sufficiently large (Region III), very few charges can transfer between the

www.MaterialsViews.com

ADVANCED
FUNCTIONAL
MATERIALS
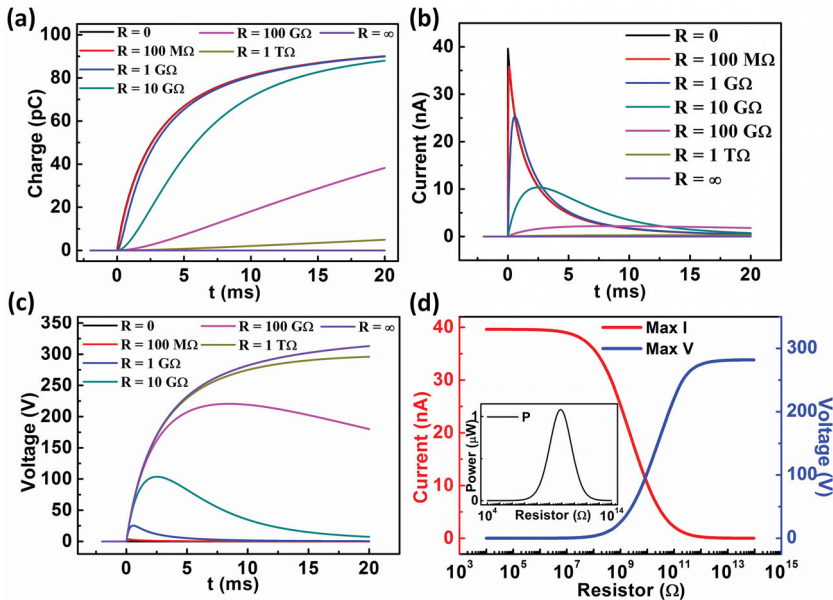www.afm-journal.de

FULL PAPER

Figure 2. Load characteristics of the conductor-to-dielectric contact-mode SETENGs. a) Transferred charge–time relationship at different load resistances. b) Current–time relationship at different load resistances. c) Voltage–time relationship at different load resistances. d) The influence of the load resistance on the maximum output current and voltage. The inset is the maximum output power profile with load resistance.

electrodes. Therefore, the output property is similar to the open circuit condition.

Given a lot of similarities between the SETENG and paired electrode TENGs, they still have a few differences both structurally and electrically. Among all of the differences, the influences of the electrode gap distance and their area size on the output performance are most important ones and need to be systematically discussed.

2.1.1. Effect of Electrode Gap Distance

Unlike paired electrode TENGs, SETENGs have a fixed gap between their two electrodes, which are independent of the motion of Dielectric 1. This leads to an approximately fixed C_0, which is critical to the performance of the whole device. To understand its influence, the fundamental properties of the SETENG, that is, V_{OC} and Q_{SC}, are calculated for SETENGs with different gap distances (g), as shown in **Figure 3**a,b. In this calculation, all of the other parameters used are the same as shown in Table 1 except the gap distance, which is specified in each figure. At the same moving distance (x), V_{OC} rises up monotonically with the increase of g while Q_{SC} decreases. When g is large enough, the raise speed V_{OC} is quite slow and V_{OC} approaches to its saturation value. Similarly, when g approaches to 0, Q_{SC} also approaches to its saturation value, as shown in Figure S2, Supporting Information.

This influence of g can be interpreted utilizing the equivalent circuit built above. When g increases, C_b and C_0 decreases significantly while C_a is barely affected. Therefore, C_2 and C_3 decrease significantly while C_1 maintains almost the same value. In addition, the decrease of C_3 is in a higher rate than that

of C_2. Therefore, from Equations 14–16, V_{OC} monotonically increases with the increase of g while Q_{SC} monotonically decreases to 0.

Besides the basic trend of V_{OC} and Q_{SC}, their saturation behavior can be theoretically understood as well. First, the saturation behavior of V_{OC} when g is sufficiently large is discussed. When g is sufficiently large, C_b and C_0 approach to 0 at the same rate while C_a is almost unaffected. Therefore, C_2 and C_3 approach to 0 with its ratio approaching to 1 while C_1 approaches to C_a. (Detailed derivation is shown in Supporting Information, Section 3.) Thus, V_{OC} can be given by the following equation, which clearly shows the saturation behavior of V_{OC} when g is large enough.

$$V_{OC}(g = \infty) = \frac{\sigma w l}{2 C_a} \qquad (24)$$

The saturation behavior of Q_{SC} can also be interpreted. When g decreases to 0, C_0 is getting close to infinity and C_a equals to C_b. Thus, both C_1 and C_2 are approaching to $C_a/2$. (Detailed derivation is shown in Supporting Information, Section 3.) As a result, Q_{SC} approaches to its saturation value $\sigma w l/2$.

Besides the fundamental property, the influence of the gap on the load characteristics is investigated as well. Utilizing Equations 20–22 and the moving-mode shown in Equation 18, the output current, voltage, and transit power peak were calculated under different load resistances for SETENGs with different g, as shown in Figure 3c–e. Consistent with what we discussed above, a smaller gap provides a higher current but a lower voltage. Therefore, Region II shifts to smaller range, leading to the decrease of the optimum resistance.[16] The relationship between the maximum transit power and the gap distance is plotted in Figure 3f. An optimum gap about 1.54 cm is observed to generate the maximized transit power.

2.1.2. Effect of Area Size (Length)

Besides the gap between the electrodes, another important design parameter is the area size (represented by the length l in this 2D model) of the SETENG. To systematically study its influence, V_{OC}, Q_{SC}, and η_{CT} of the SETENG with different length l is calculated through the COMSOL software, as shown in **Figure 4**a–c. All of the parameters utilized in this calculation are listed in **Table 2**. From the calculation results, for any given x, there exists a specific l to generate the largest V_{OC}. In addition, when x increases, this l for the largest V_{OC} also increases. Q_{SC} should have been proportional to the length l, but this is true only when l is sufficiently small. When l is large enough, the Q_{SC}-l curve shifts downwards dramatically, which shows that η_{CT} decreases significantly when l is large.
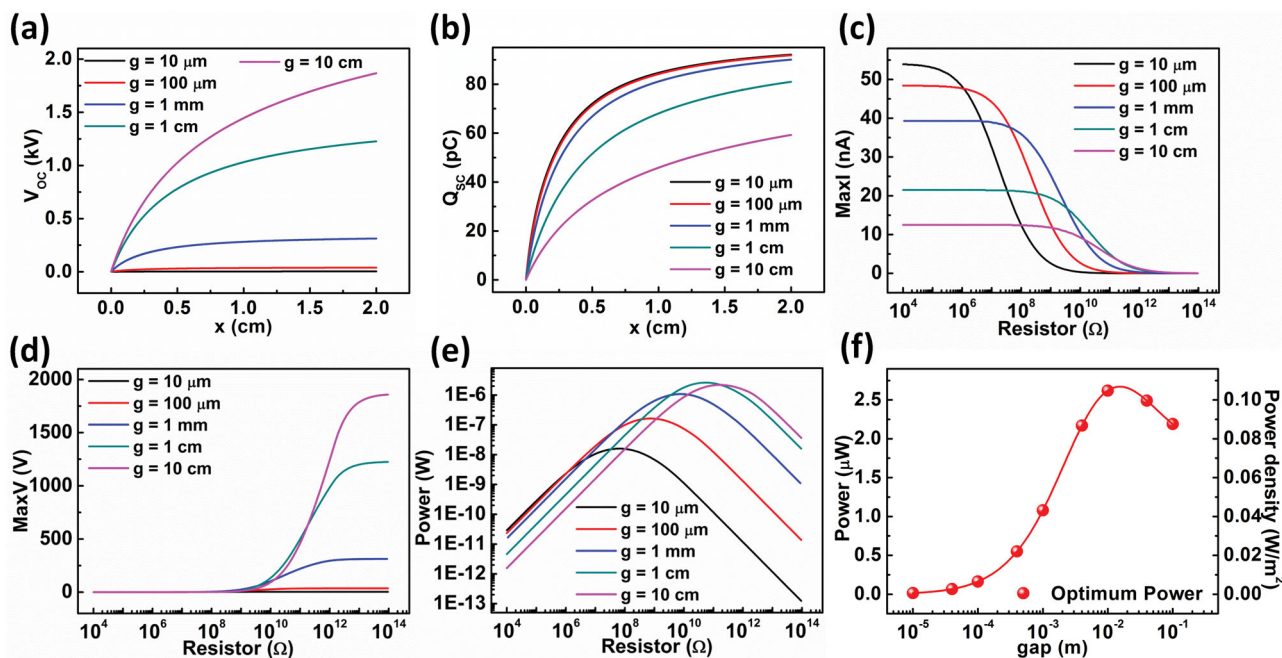
Figure 3. The influence of electrode gap distance (*g*) on the output characteristics of the conductor-to-dielectric contact-mode SETENGs. a) The relationship between open circuit voltage and separation distance at different gap distances. b) The relationship between transferred charges at short circuit and separation distance at different gap distance. c–e) Maximum output c) current profile, d) voltage profile, and e) power profile with load resistance at different gap distances. f) Extracted optimum power profile with electrode gap distance.

The complicate behavior of the influence of *l* to outputs of SETENGs can be understood from the equivalent circuit built above. The capacitances C_a, C_b, and C_0 are first calculated, which are all 2D parallel electrode capacitances. For an non-ideal 2D parallel electrode capacitance considering the edge effect, its capacitance value can be shown as the following equation,[18]
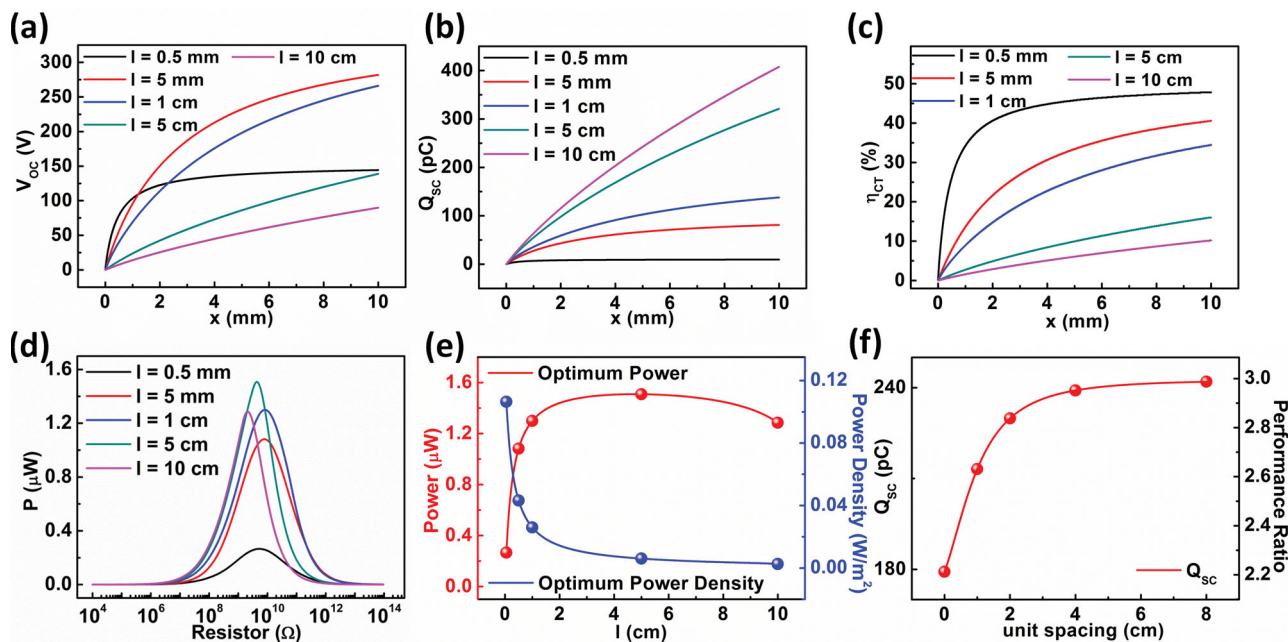

Figure 4. The influence of area size (length) on the output characteristics of the conductor-to-dielectric contact-mode SETENGs. a) Open circuit voltage profiles with separation distances for SETENGs with different lengths. b) Short circuit transferred charges profile with separation distances for SETENGs with different lengths. c) Short circuit charge transfer efficiency profile with separation distances for SETENGs with different lengths. d) Maximum output power profile with load resistance for SETENGs with different lengths. e) Extracted optimum power and power density profile with length of SETENG. f) The influence of unit spacing on the short circuit transferred charges in a three-SETENG system.

www.MaterialsViews.com

ADVANCED
FUNCTIONAL
MATERIALS
www.afm-journal.de

FULL PAPER

Table 2. Parameters utilized in the calculation of SETENG's output properties with different l.

Dielectric 1	$\varepsilon_{r1} = 2$, $d_1 = 100$ μm
Thickness of electrodes d_m	1 μm
Width of the structrue w	5 mm
Gap distance between electrodes g	1 mm
Tribo-charge surface density σ	8 μC m^{-2}
Maximum separation distance x_{max}	0.01 m
Average Velocity v	1 m s^{-1}

$$C = \frac{\varepsilon_0 wl}{d}\left\{1 + \frac{d}{\pi l}\left\{1 + \ln\left[1 + \frac{2\pi l}{d} + \ln\left(1 + \frac{2\pi l}{d}\right)\right]\right\}\right\}$$
$$= \frac{\varepsilon_0 wl}{d}\left[1 + \alpha\left(\frac{d}{l}\right)\right] \tag{25}$$

where l is its length, w is its width and d is the separation distance between the two parallel electrodes. Inside Equation 25, the edge effect is reflected by the function $\alpha(\gamma)$:

$$\alpha(\gamma) = \frac{\gamma}{\pi}\left\{1 + \ln\left[1 + \frac{2\pi}{\gamma} + \ln\left(1 + \frac{2\pi}{\gamma}\right)\right]\right\} \tag{26}$$

With C_a, C_b, and C_0 calculated through the above equation, C_1, C_2, and C_3 can be analytically calculated utilizing Equations 8–10. Thus, from the calculated C_1, C_2, and C_3, V_{OC}, Q_{SC}, and η_{CT} can be analytically calculated through Equations 14–16. Their behaviors at the two l limits are shown below. (Detailed derivation is shown in Supporting Information, Section 4.)

When l approaches to 0 (x/l and g/l is very large):

$$V_{OC} = \frac{\sigma}{2\varepsilon_0}\pi l \tag{27a}$$

$$Q_{SC} = \frac{\sigma wl}{2} \tag{27b}$$

$$\eta_{CT} = \frac{1}{2} \tag{27c}$$

When l approaches to infinity (x/l and g/l is close to 0):

$$V_{OC} = \frac{\sigma g\, x\, \ln(l)}{\pi\varepsilon_0 l} \tag{28a}$$

$$Q_{SC} = \frac{\sigma wx}{\pi}\ln(l) \tag{28b}$$

$$\eta_{CT} = \frac{x}{\pi l}\ln(l) \tag{28c}$$

From Equations 27a and 28a, the behavior of V_{OC} can be quite easily understood. When l is small, V_{OC} is proportional to l and increase with the increase of l. But when l is large enough, V_{OC} satisfies Equation 28a and starts to drop. Therefore, there is an optimum l at which V_{OC} reaches its maximum. When x

or g increases, a larger range of l can satisfy the condition for Equation 27, so that the l providing the maximum V_{OC} rises. For Q_{SC}, when l is small (condition of Equation 27), Q_{SC} is proportional to l and increases dramatically with the increase of l. When l is sufficiently large (condition of Equation 28), Q_{SC} is proportional to $\ln(l)$, resulting in a much lower slope of Q_{SC}-l curve. From the Q_{SC} behavior, η_{CT} is close to 50% when l is small and decays to 0 when l is sufficiently large. This analysis clearly explains the FEM calculation results shown in Figure 4.

Besides these fundamental characteristics, the load characteristics of the contact-mode SETENG are studied as well. Because V_{OC} and η_{CT} of SETENGs with infinite l are 0, an optimum l of 4.7 cm is observed to generate the maximum total transit power, as shown in Figure 4d,e. In addition, the optimum resistance increases first then starts to decrease when l increases. This is because when l first increases, V_{OC} increases at a faster speed than I_{SC}, Region II of the single electrode shifts to a higher resistance range and the optimum resistance increases.[16] When l further increases, V_{OC} starts to decrease and I_{SC} continues increasing. Thus, the optimum resistance starts to decrease.[16] Moreover, the peak power density is monotonically lowered when l increases, which is because larger area l lower η_{CT}. Thus, unlike the paired electrode TENGs, SETENGs are not optimized for direct scaled-up processing.

2.1.3. Effect of Unit Spacing for Scale Up

Finally, the effect of connecting several SETENGs in parallel is discussed, which is another way to scale-up the output from SETENGs besides increasing the area size. For a three-SETENG system, a simulation was performed at OC condition through FEM calculation, in order to study the influence of the spacing between each SETENG (Figure S3, Supporting Information). The total Q_{SC} generated by the three SETENGs with different spacing is shown in Figure 4f. When the unit spacing is small, electric field from each SETENG will interfere, resulting in a decrease of η_{CT} for each SETENG, which is similar to the effect of increasing l on one SETENG. Only when their spacing is large enough, the mutual influence will be minimized, so that there will be little decrease on η_{CT}. From Figure 4f, to reach the total charge transfer amount more than 270% of that for each SETENG, a minimum unit spacing of 1.24 cm is observed, about 2.5 times the length of an individual SETENG. Therefore, a large enough spacing is critical for the scale-up of the output through parallel connection.

2.2. Dielectric-to-Dielectric Contact-Separation Mode SETENGs

Other than conductor-to-dielectric SETENGs, dielectric-to-dielectric SETENGs of contact-mode are investigated as well. The basic FEM model of dielectric-to-dielectric SETENGs is shown in **Figure 5**a. The only difference of this structure is that another layer of dielectric (Dielectric 2) is utilized as the counter tribo-layer on top of the primary electrode. The FEM calculation results at OC condition show a similar electric field distribution compared to that of the conductor-to-dielectric contact-mode SETENGs, as provided in Figure 5b. This leads to a similar
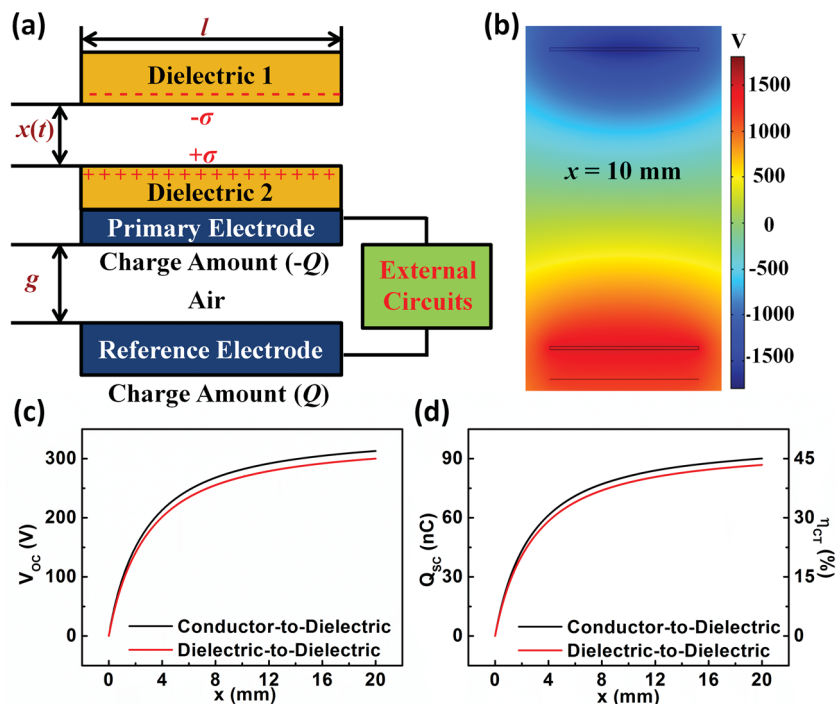
Figure 5. Characteristics of dielectric-to-dielectric contact-mode SETENGs. a) Structure of the FEM model. b) Calculated electric potential distributions at different moving distances x. c,d) Calculated c) open circuit voltage, and d) transferred charges at short circuit condition of SETENGs at different *x*, together with comparison with results of corresponding conductor-to-dielectric contact-mode SETENGs.

open circuit voltage profile and short circuit charge profile, with only a little decrease in magnitude, as shown in Figure 5c,d. This decrease in magnitude is because of the thickness of Dielectric 2. Similar to that in the paired-electrode TENG,[15,16] the conductor-to-dielectric mode can be thought the same as the dielectric-to-dielectric mode at the limit of zero Dielectric 2 thickness. Since the thickness of the dielectric film is much smaller than its length in practical situation, its performance will be quite close to that in conductor-to-dielectric contact-mode SETENGs. Therefore, all the discussions in the conductor-to-dielectric SETENGs, such as the load characteristics and the influence of structural parameters, are applicable to dielectric-to-dielectric SETENGs.

3. Sliding-Separation Mode SETENGs

Besides the contact-mode SETENGs, there is another mode of SETENGs that is based on in-plane charge separation, called sliding-mode SETENGs. First, the conductor-to-dielectric sliding-mode SETENG is investigated. Its basic output characteristics (V_{OC} and Q_{SC}) are quite similar to that of the contact-mode SETENG, as shown in **Figure 6**a,b.
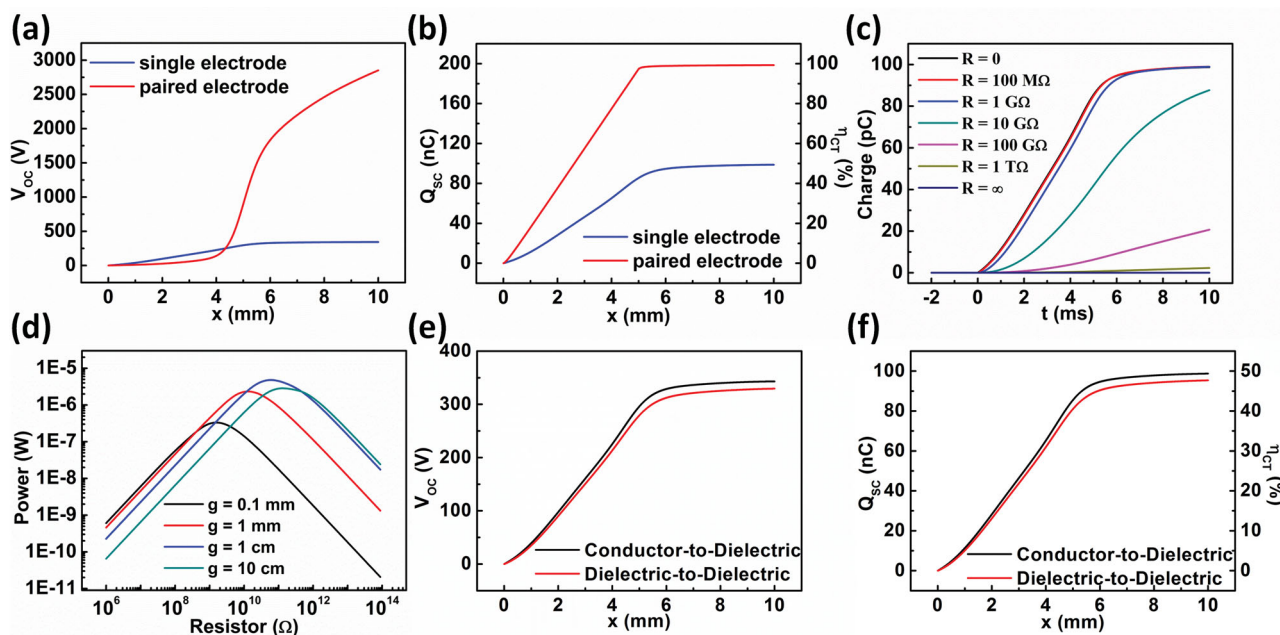

Figure 6. Characteristics of the sliding-mode SETENGs. a,b) Calculated a) open circuit voltage, and b) transferred charges at short circuit condition of conductor-to-dielectric category SETENGs at different *x*, together with comparison with results of paired electrode TENGs. c) Transferred charge-time relationship at different load resistances for conductor-to-dielectric category. d) Maximum output power profile with load resistance at different gap distances for conductor-to-dielectric category. e,f) Calculated e) open circuit voltage, and f) transferred charges at short circuit condition of dielectric-to-dielectric SETENGs at different *x*, together with comparison with results of corresponding conductor-to-dielectric sliding-mode SETENGs.

www.MaterialsViews.com

ADVANCED
FUNCTIONAL
MATERIALS
www.afm-journal.de

FULL PAPER

The maximum possible η_{CT} is also 50%, but this value can be approached at a much smaller x. This is because when Dielectric 1 is completely separated from the primary electrode, C_a is mainly from the side capacitance and decreases dramatically with the increase of x. In addition, the electrostatic shielding effect of the primary electrode is relatively small in this mode. As a typical property of SETENG, the three-working-region behavior is also observed, as shown in Figure 6c. The influence of the gap on its optimum performance is quite similar to the contact-mode TENG. A larger gap will provide a higher V_{OC} but a lower Q_{SC}. Thus, there exists an optimum gap for an optimum power output, as shown in Figure 6d. The comparison between the output characteristics of conductor-to-dielectric sliding-mode SETENG and dielectric-to-dielectric sliding-mode SETENG is shown in Figure 6e,f. Similar to contact-mode SETENGs, their V_{OC} and Q_{SC} profiles are alike to each other, resulting in the same load characteristics.

4. Conclusion

In summary, a theoretical model of SETENGs is presented, which is the first in-depth interpretation and analysis of the SETENG's working principle, clearly showing its unique operation characteristics. The capacitance effect from the direct electric field line connecting between the dielectric and the reference electrode (without electrostatic shield effect of the primary electrode) was the core factor determining the physics behavior of SETENGs. On the basis of this analysis, the impacts of two important structural parameters, that is, the electrode gap distance and the area size, on the output performance were theoretically investigated. First, increasing electrode gap distance will lead to monotonic increase of the V_{OC} and decrease of the Q_{SC}, indicating there exists an optimum electrode gap distance to obtain maximum power output; second, the expansion of area size will affect the charge transfer efficiency, leading to an optimum length at which the transit output power is optimized. In addition, parallel connection of multiple SETENGs with micro-scale size and relatively larger spacing should be utilized as the scaling-up strategy. Sliding-mode SETENGs behaves similarly as contact-mode SETENGs, but a full separation is sufficient to reach a relative high charge transfer efficiency that is close to 50%. The discussion of the influence of structural parameters on the whole performance of the device can serve as an important guidance for rational design of the device structure towards the optimum output in specific applications.

Supporting Information

Supporting Information is available from the Wiley Online Library or from the author.

Acknowledgements

[1] L. S. McCarty, G. M. Whitesides, *Angew. Chem., Int. Ed.* **2008**, *47*, 2188.
[2] R. G. Horn, D. T. Smith, A. Grabbe, *Nature* **1993**, *366*, 442.
[3] H. T. Baytekin, A. Z. Patashinski, M. Branicki, B. Baytekin, S. Soh, B. A. Grzybowski, *Science* **2011**, *333*, 308.
[4] F. R. Fan, Z. Q. Tian, Z. L. Wang, *Nano Energy* **2012**, *1*, 328.
[5] G. Zhu, Z. H. Lin, Q. S. Jing, P. Bai, C. F. Pan, Y. Yang, Y. S. Zhou, Z. L. Wang, *Nano Lett.* **2013**, *13*, 847.
[6] S. H. Wang, L. Lin, Y. N. Xie, Q. S. Jing, S. M. Niu, Z. L. Wang, *Nano Lett.* **2013**, *13*, 2226.
[7] S. H. Wang, Y. N. Xie, S. M. Niu, L. Lin, Z. L. Wang, *Adv. Mater.* **2014**, DOI: 10.1002/adma.201305303
[8] Y. F. Hu, J. Yang, Q. S. Jing, S. M. Niu, W. Z. Wu, Z. L. Wang, *ACS Nano* **2013**, *7*, 10424
[9] S. H. Wang, L. Lin, Z. L. Wang, *Nano Lett.* **2012**, *12*, 6339.
[10] Y. S. Zhou, G. Zhu, S. M. Niu, Y. Liu, P. Bai, Q. S. Jing, Z. L. Wang, *Adv. Mater.* **2014**, DOI: 10.1002/adma.201304619.
[11] Y. Yang, Y. S. Zhou, H. L. Zhang, Y. Liu, S. Lee, Z. L. Wang, *Adv. Mater.* **2013**, *25*, 6594.
[12] B. Meng, W. Tang, Z. H. Too, X. S. Zhang, M. D. Han, W. Liu, H. X. Zhang, *Energy Environ. Sci.* **2013**, *6*, 3235.
[13] F. Saurenbach, D. Wollmann, B. D. Terris, A. F. Diaz, *Langmuir* **1992**, *8*, 1199.
[14] L. H. Lee, *J. Electrostat.* **1994**, *32*, 1.
[15] S. M. Niu, Y. Liu, S. H. Wang, L. Lin, Y. S. Zhou, Y. F. Hu, Z. L. Wang, *Adv. Mater.* **2013**, *25*, 6184.
[16] S. M. Niu, S. H. Wang, L. Lin, Y. Liu, Y. S. Zhou, Y. F. Hu, Z. L. Wang, *Energy Environ. Sci.* **2013**, *6*, 3576.
[17] J. Stoer, R. Bulirsch, Introduction to numerical analysis, Springer, New York **2002**.
[18] Y. Li, Y. H. Li, Q. X. Li, Y. Y. Zi, *J. Tsinghua Univ. (Sci. & Tech.)* **2003**, *43*, 1024.